

**NOVEL BILE ACID AND DIPYRROMETHANE BASED
RECEPTORS FOR ION AND FLAVIN RECOGNITION**

PRADEEP KUMAR MUWAL



**DEPARTMENT OF CHEMISTRY
INDIAN INSTITUTE OF TECHNOLOGY DELHI
AUGUST, 2015**

© Indian Institute of Technology Delhi (IITD), New Delhi, 2015

**NOVEL BILE ACID AND DIPYRROMETHANE BASED
RECEPTORS FOR ION AND FLAVIN RECOGNITION**

by

PRADEEP KUMAR MUWAL

Department of Chemistry

Submitted

in fulfillment of the requirements of the degree of

Doctor of Philosophy

to the



INDIAN INSTITUTE OF TECHNOLOGY DELHI

August, 2015

This thesis is dedicated to Sai Baba and my parents

CERTIFICATE

This is to certify that the thesis entitled, “**Novel Bile Acid and Dipyrrromethane Based Receptors for Ion and Flavin Recognition**”, being submitted by Mr. Pradeep Kumar Muwal, to the Indian Institute of Technology Delhi, for the award of the degree of ‘Doctor of Philosophy in Chemistry’, is a record of bonafide research work carried out by him. Mr. Pradeep Kumar Muwal has worked under my guidance and supervision and has fulfilled all the requirements for the submission of this thesis, which to my knowledge has reached the requisite standard. The results embodied in this thesis have not been submitted in part or in full, to any other University or Institute for award of any degree or diploma.

Prof. Pramod S. Pandey

(Thesis Supervisor)

Professor

Department of Chemistry

Indian Institute of Technology Delhi

New Delhi-110016

INDIA

ACKNOWLEDGEMENTS

This thesis is the result of almost five years of work whereby I have been accompanied and supported by many people. It is a pleasure that I now have the opportunity to express my gratitude for all of them.

Words cannot do justice in expressing my immense pleasure and profound gratitude towards my research supervisor **Professor P. S. Pandey**, Department of Chemistry, IIT Delhi, who has always been caring and insightful sources of knowledge and encouragement. I would like to take this opportunity to express my sincere gratitude to him for not only allowing me to accomplish research under his guidance, but also for encouraging me to think independently and develop a scientific attitude with utter patience and enthusiasm. He continually and convincingly conveyed a spirit of adventure in regard to research and an excitement in regard to learning.

I would also like to thank all the past and present heads of the departments of Chemistry, IIT Delhi for providing me necessary facilities required for the completion of this research work. I would also like to acknowledge the official staff of the departments, Mr. Kesav Dev, Munna Lal, Virendra Sharma, J. P. Sharma and other staffs.

I would like to offer my sincer thanks to Dr. Shubha Pandey for the fluorescence studies and Dr. Roli Mishra for help in synthesis of some compounds. I am thankful to my seniors, Dr. Prosenjit Chattopadhyay, Dr. Anjul Kumar, Dr. Anamica Tripathi, Dr. Rajesh Kumar Chhatra and Dr. Aradhana Nayal for their moral support and critical comments during the progress of the research work.

I would like to extend my heartfelt thanks to my friends Dr. Jitender Sharma, Dr. Akhil Badjatiya, Md. Atiqullah, Dr. Anil Malik, Dr. Vedvati Singh, Kamal Nayan Sharma, Dharendra Yadav, Ashima Malik, Tanu Gupta, Preeti, Hemant Sharma, Dheeraj Kumar, Rahul Siwatch, Mahendra Sharma, Surendra Kumar, Amit Soni, Siddhart Sirohi, Vineet, and all other friends whose name are not listed here, for their best wishes, support, and inspiration during my stay at IIT Delhi.

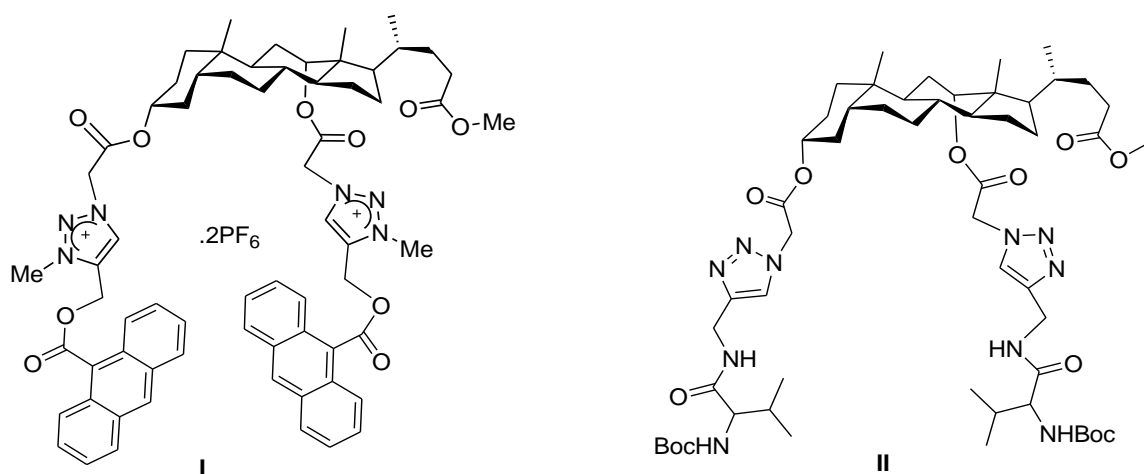
Last, but not the least, I would like to offer my sincere regards to all members of my family for their patience, support and constant encouragement. I would like to offer sincere thanks to my father Kishna Ram, my mother Mrs. Rashmi, my late grandfather, my grandmother, my uncle, my aunty, my father-in-law J. P. Choudhary, my mother-in-law Kamla Choudhary and my dearest brothers Rajesh Muwal, Anil Muwal, Rajendra Muwal, Harendra Muwal for their moral support and invaluable advice during some of the most difficult and demanding moments of my life. I also offer my special thanks to my wife, Komal Choudhary, for not only all her help during this work but for her understanding and love during the past few years. Her support and encouragement was in the end what made this dissertation possible. In the end, I must extend my sincere thanks to the Council of Scientific and Industrial Research (CSIR), Government of India, for the award of Senior Research Fellowship.

Pradeep Kumar Muwal

ABSTRACT

The present thesis deals with the synthesis of steroidal and non-steroidal receptors and studies of their binding properties towards ions and a flavin derivative. It also focuses on the design and synthesis of a dipyrromethane-based receptor and studies of its ion recognition properties. The thesis has been divided into five chapters.

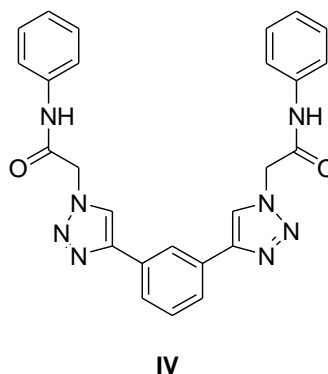
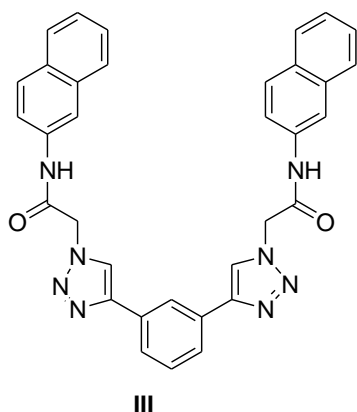
The first chapter presents a brief literature survey on ion recognition based on bile acids and dipyrromethane scaffolds and on 2,4-diaminopyridine-based flavin receptors. The second chapter describes the synthesis and ion recognition properties of steroidal and non-steroidal receptors. Deoxycholic acid-based 1,2,3-triazolium acyclic receptor **I** and 1,2,3-triazole receptor **II** were synthesized and their anion recognition property has been studied.



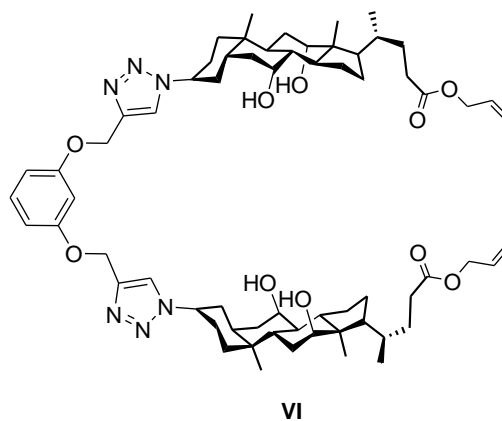
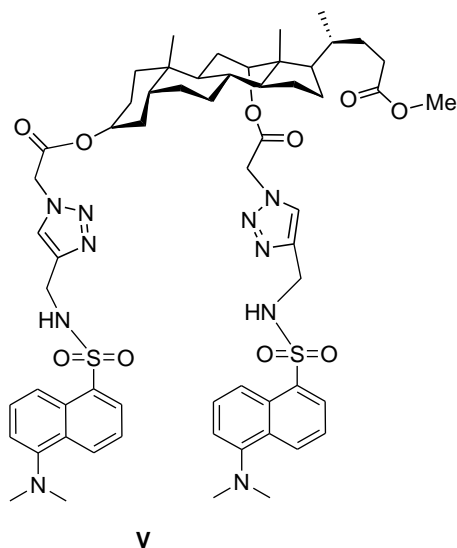
The anion binding property of the bile acid-based receptors **I** and **II** was examined in chloroform by ¹H NMR titration. Both receptors showed the highest affinity for acetate ion with an association constant of about 1500 M⁻¹ and 1480 M⁻² respectively. The observed selectivity trend was CH₃COO⁻ > Cl⁻ > Br⁻ > F⁻ > HSO₄⁻ > I⁻. Receptor **I** also showed precipitation behavior with H₂PO₄⁻ ion in acetonitrile.

The synthesis and anion binding behavior of non-steroidal receptors **III** and **IV**, containing 1,2,3-triazole as well as amide moieties have also been described. Receptors **III** and **IV** showed high selectivity for dihydrogen phosphate ion with a binding constant of 400 M⁻¹ and

180 M⁻¹, respectively. The observed selectivity trend in both cases was H₂PO₄⁻ > CH₃COO⁻ > F⁻ > Cl⁻ > Br⁻.

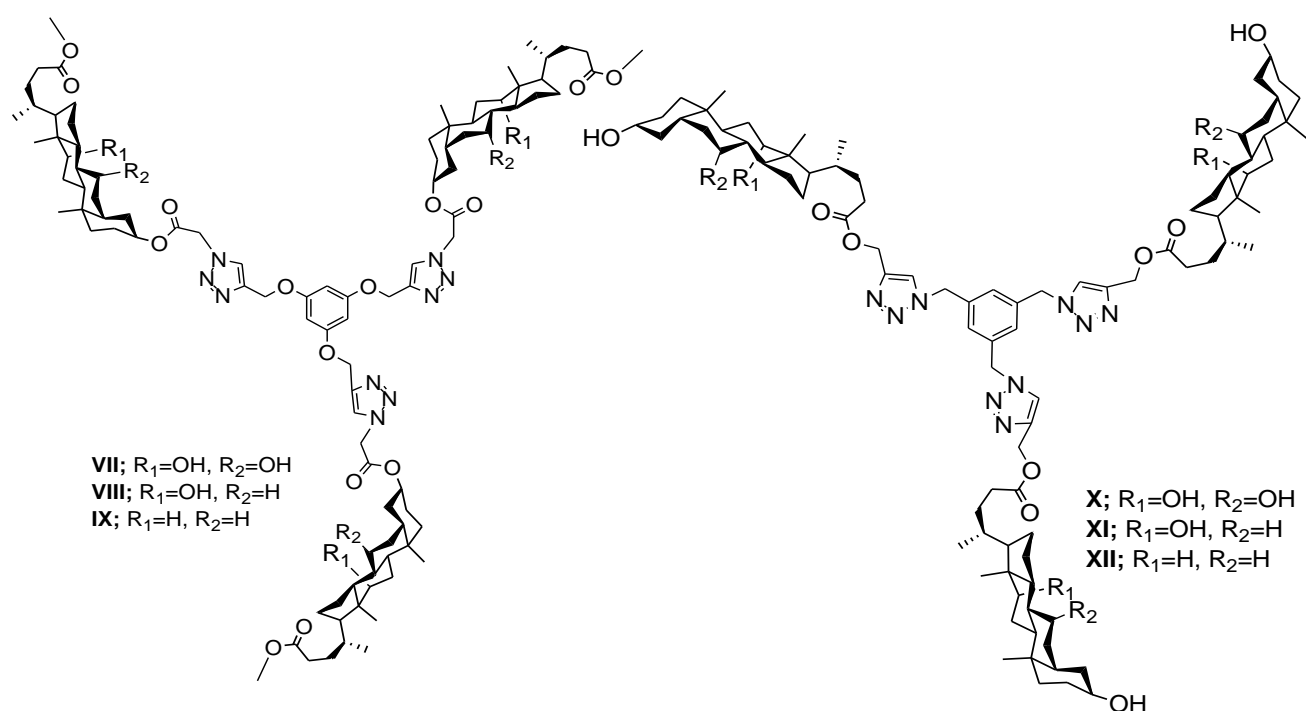


This chapter also deals with the synthesis of bile acid-based 1,2,3-triazole receptors **V** and **VI** for the recognition of metal ions. The binding behavior of the receptor **V** towards metal ions was studied in CHCl₃:MeOH (7:3, v/v) by molecular fluorescence and UV-Vis titration. Receptor **V** showed very high selectivity for Hg²⁺ ion with a binding constant of 3.3×10⁴ M⁻¹. However, compound **VI** was found to be selective for Cu²⁺ metal ion. Receptor **VI** also showed precipitate formation with Hg²⁺ ion in CHCl₃:MeOH (7:3, v/v).



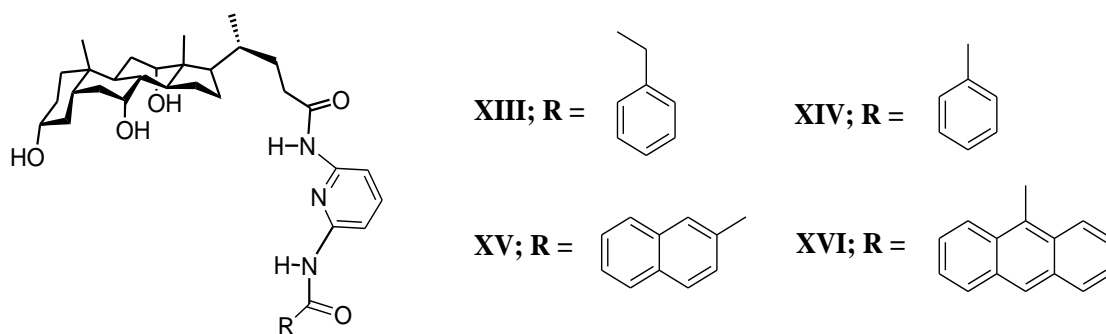
The third chapter deals with the synthesis of 1,2,3-triazole containing tripodal receptors **VII-XII**, their application in stabilization of silver nanoparticles and their ion-sensing properties. An efficient method for the synthesis of silver nanoparticles has been developed through the

stabilization of nanoparticles with tripodal compounds **VII-XII** under visible light. These nanoparticles have been used for the colorimetric sensing of transition metal ions and anions. All of these nanoparticles showed remarkably selective colorimetric sensing for Hg^{2+} ion. As for the anion sensing, silver nanoparticles stabilized with **VIII** and **IX** showed the colorimetric response for both H_2PO_4^- and NO_3^- ions. However, silver nanoparticles stabilized with compounds **XI** and **XII** were found to be sensitive only for H_2PO_4^- ion.

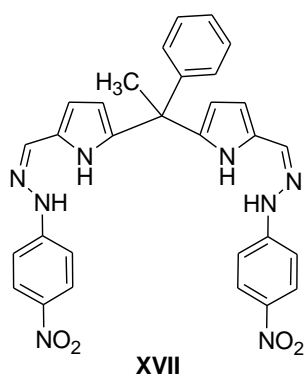


The fourth chapter describes the synthesis of bile acid-based receptors **XIII-XVI** containing 2,6-diaminopyridine unit and their binding studies with a flavin analogue. Flavoproteins containing flavin cofactors FAD (flavin adenine dinucleotide) or FMN (flavin mononucleotide) catalyze a variety of biological redox transformations. 2,6-Diaminopyridine derivatives have been found to bind flavin derivatives through three hydrogen bonds. The binding properties of the bile acid-based receptors **XIII-XVI** with *N*(10)-hexylflavin were examined in chloroform by ^1H NMR titration. It was observed that there was significant aromatic π -stacking interaction between the flavin ring and the aromatic unit of these

receptors along with the hydrogen bonding interaction with amide protons. The binding constants for **XIII**, **XIV** and **XV** were found to be 3500, 2000 and 1000 M⁻¹, respectively. In the case of **XVI**, very little change in the chemical shift of amide and other protons was observed. The unexpected decrease in the binding of **XVI**, may be due to the steric hindrance arising from the anthracene ring preventing the N-H--X hydrogen bond interaction.



The fifth chapter deals with the synthesis of a dipyrromethane-based receptor **XVII** and its ion recognition properties. The binding behavior of receptor **XVII** towards metal ions was studied in acetonitrile by UV-Vis titration. It showed very high selectivity for fluoride and copper ions with binding constants of 6.02×10^3 and 9.82×10^3 M⁻¹, respectively. It also showed the colorimetric change with fluoride and copper ions.



CONTENTS

	Page No.
Certificate	i
Acknowledgements	ii
Abstract	iv
List of Figures	viii
List of Tables	xx
Glossary of Symbols and Abbreviation	xxi
Notes	xxiii
CHAPTER I: Introduction.	
1.1 Introduction	1
1.2 Bile acid-based receptors for ion recognition	1
1.3 Flavin receptors based on 2,6-diaminopyridine	10
1.4 Dipyrrromethane-based receptors for anion recognition	14
References	20
CHAPTER 2: Synthesis and ion recognition properties of bile acid-based receptors	
2.1 Introduction	25
2.1.1 1,2,3-Triazole based receptors for anion recognition	26
2.1.2 1,2,3-Triazolium based receptors for anion recognition	35
2.1.3 1,2,3-Triazole based receptors for metal ions recognition	40
2.2 Present Study	52
2.3 Results and discussion	53
2.3.1 Bile acid-based anion receptors	53
2.3.1.1 Synthesis of bile acid-based acyclic 1,2,3-triazolium receptor	53

2.3.1.2 Anion binding studies of receptor 89 using ^1H NMR titration	55
2.3.1.3 Anion precipitation studies of receptor 90 -(PF ₆) ₂ salt	58
2.3.1.4 Synthesis of bile acid-based acyclic 1,2,3-triazole receptor 93 Containing amide groups	60
2.3.1.5 Anion binding studies of receptor 93 using ^1H NMR titration	61
2.3.1.6 Synthesis of non-steroidal 1, 2, 3-triazole receptors containing amide groups	63
2.3.1.7 Anion binding studies of receptors 97a and 97b using ^1H NMR titration	65
2.3.2 Bile acid based metal ion receptors	67
2.3.2.1 Synthesis of dansyl appended bile acid-based receptor	67
2.3.2.2 Synthesis of bile acid-based acyclic receptor 105	69
2.3.2.3 Metal ion binding studies of receptor 100 using fluorescence and UV-Vis titration	71
2.3.2.4 Metal ion binding studies of receptor 105 using UV-Vis titration	78
2.3.2.5 Metal precipitation studies of receptor 105	79
2.4 Conclusion	81
2.5 Experimental details	83
References	115
 CHAPTER 3: Synthesis of 1,2,3-triazole containing tripodal receptors, their application in stabilization of silver nanoparticles and their ion- sensing properties	
3.1 Introduction	122
3.1.1 Colorimetric sensing of metal ions by nanoparticles	122
3.1.2 Colorimetric sensing of anions by nanoparticles	128

3.2 Present study	131
3.3 Results and discussion	132
3.3.1 Synthesis of bile acid-based 1,2,3-triazole containing tripodal ligands	132
3.3.2 Synthesis of 1,2,3-triazole-stabilized silver nanoparticles	136
3.3.3 Application of 1,2,3-triazole-stabilized silver nanoparticles in colorimetric detection of metal ions and anions	138
3.4 Conclusion	143
3.5 Experimental details	144
References	170
CHAPTER 4: Synthesis of bile acid-based receptors containing 2,6-diaminopyridine unit and their binding studies with a flavin analogue	
4.1 Introduction	172
4.2 Present Study	176
4.3 Results and discussion	177
4.3.1 Synthesis of bile acid-based acyclic flavin receptors	177
4.3.2 Binding studies of receptors with <i>N</i> (10)-hexylflavin using ¹ H NMR titration	179
4.4 Conclusion	184
4.5 Experimental details	185
References	199
CHAPTER 5: Synthesis and ion recognition properties of a dipyrromethane-based receptor	
5.1 Introduction	201
5.2 Present Study	203
5.3 Results and discussion	203

5.3.1 Synthesis of the dipyrromethane-based receptor	203
5.3.2 Anion-recognition studies and anion sensing properties of dipyrromethane based receptor 14	205
5.3.3 Metal binding and metal sensing properties of dipyrromethane based receptor 14	209
5.4 Conclusion	211
5.5 Experimental details	212
References	218
Bio-data of the author	220

LIST OF FIGURES

Figure No.	Description	Page No.
Figure 2.1	Hydrogen bond donor and acceptor sites in 1,2,3-triazole and triazolium ring mechanism of click reaction	25
Figure 2.2	(a) Partial ^1H NMR titrations stacking plot of receptors 90 (10 mM, CDCl_3 , 298 K) with increasing equivalent of acetate ion (0-5.8 equiv.) from bottom to the top (b) Proposed binding mode between receptor 90 and acetate ion.	57
Figure 2.3	(a) ^1H NMR titration binding isotherm for receptor 90 and acetate ion in CDCl_3 ($K_a = 1500 \text{ M}^{-1}$). (b) Job's plot showing 1:1 complex formation between 90 and acetate ion.	58
Figure 2.4	(a) Solution of receptor (10mM) in CD_3CN (b) Precipitate formed by receptor with TBAH_2PO_4 (1.8 mM)	58
Figure 2.5	Partial ^1H NMR titrations stacking plot of receptor 90 (10 mM, CDCl_3 , 298 K) with increasing equivalent of TBA dihydrogen phosphate (0-3.6 equiv.) from bottom to the top	59
Figure 2.6	(a) ^{31}P NMR spectrum of PF_6 salt of receptor 90 ; (b) ^{31}P NMR spectrum of precipitate; (c) ^{19}F NMR spectrum of PF_6 salt of receptor 90	60
Figure 2.7	(a) SEM image of PF_6 salt of receptor 90 (b) SEM image of precipitate formed by receptor 90 in the presence of H_2PO_4^-	60

Figure 2.8	(a) Partial ^1H NMR titrations stacking plot of receptors 93 (10 mM, CDCl_3 , 298 K) with increasing equivalent of acetate anion (0-6.2 equiv.) from bottom to the top (b) Proposed binding mode between receptor 93 and acetate ions.	62
Figure 2.9	(a) ^1H NMR titration binding isotherm for receptor 93 and acetate ion in CDCl_3 ($K_a = 1480 \text{ M}^{-2}$). (b) Job's plot showing 1:2 complex formations between 93 and acetate ion.	63
Figure 2.10	(a) ^1H NMR titration binding isotherm for receptor 97a and dihydrogen phosphate ion in 20% DMSO in CDCl_3 ($K_a = 400 \text{ M}^{-1}$). (b) Job's plot showing 1:1 complex formation between 97a and dihydrogen phosphate ion	66
Figure 2.11	^1H NMR titration binding isotherm for receptor 97b and dihydrogen phosphate ion in 20% DMSO in CDCl_3 ($K_a = 180 \text{ M}^{-1}$)	66
Figure 2.12	Quenching of fluorescence intensity of receptor 100 (25 μM) in the presence of Hg^{2+} in $\text{CHCl}_3:\text{MeOH}$ (7:3, v/v) ($\lambda_{\text{excitation}} = 351 \text{ nm}$)	72
Figure 2.13	Excited-state intensity decay curves of 100 (25 μM) in the absence (upper panel) and presence (lower panel) of 100 μM Hg^{2+} in $\text{CHCl}_3:\text{MeOH}$ (7:3, v/v)	73
Figure 2.14	Change in fluorescence intensity of 100 upon addition of Hg^{2+} for $0 \leq [\text{Hg}^{2+}] \leq 25 \mu\text{M}$ (calibration plot for the calculation of detection limit)	73

- Figure 2.15 Change in UV-Vis spectra of receptor **100** (100 μM) upon addition of Hg^{2+} in $\text{CHCl}_3:\text{MeOH}$ (7:3, v/v) 74
- Figure 2.16 Percentage reduction in the fluorescence intensity of **100** in the presence of 100 μM M^{n+} in $\text{CHCl}_3:\text{MeOH}$ (7:3, v/v) ($\lambda_{\text{excitation}} = 351 \text{ nm}$). Inset shows selectivity coefficient, 75
- $$k_{\text{M}^{n+}, \text{Hg}^{2+}} = \frac{m_{\text{M}^{n+}}}{m_{\text{Hg}^{2+}}} = \frac{\Delta F_{\text{M}^{n+}}}{\Delta F_{\text{Hg}^{2+}}} \text{ for } \mathbf{100}.$$
- Figure 2.17 % reduction in the fluorescence intensity of **100** (25 μM) in the presence of 100 μM each of M^{n+} and Hg^{2+} in $\text{CHCl}_3:\text{MeOH}$ (7:3, v/v) at ambient conditions ($\lambda_{\text{excitation}} = 351 \text{ nm}$) 76
- Figure 2.18 Change in fluorescence of **100** upon addition of Hg^{2+} for $0 \leq [\text{Hg}] \leq 200 \mu\text{M}$. 76
- Figure 2.19 Partial ^1H NMR spectra (300 MHz, $\text{CDCl}_3:\text{CD}_3\text{OD}$, (7:3, v/v), δ in ppm) of **100** showing chemical shift change in the presence of incremental addition of $\text{Hg}(\text{ClO}_4)_2 \cdot \text{H}_2\text{O}$ ($\text{CDCl}_3:\text{CD}_3\text{OD}$, (7:3, v/v)). 77
- Figure 2.20 Absorbance spectra of compound **105** ($1 \times 10^{-4} \text{ M}$) in $\text{CHCl}_3/\text{MeOH}$ (7:3, v/v) in the presence of Cu^{2+} (0-2.4 equiv). 78
- Figure 2.21 (a) Hildebrand-Benesi plot based on the 1:1 binding model: $A_0/(A-A_0)$ versus $[\text{G}]^{-1}$; (b) Jobs plot showing 1:1 complex formation between compound **105** and Cu^{2+} 79
- Figure 2.22 (a) Solution of receptor **105** (10mM) in $\text{CHCl}_3/\text{MeOH}$ (7:3, 80

	v/v) (b) Precipitate formed by receptor with Hg ²⁺ (1.8 mM)	
Figure 2.23	Absorbance spectra of compound 105 (1×10^{-4} M) in CHCl ₃ /MeOH (7:3, v/v) in the presence of Hg ²⁺ (0-3 equiv)	80
Figure 2.24	(a) SEM images of receptors 105 (b) SEM image of precipitate formed by receptor 105 in the presence of Hg ²⁺ .	81
Figure 2.25	Partial ¹ H NMR titrations stacking plot of receptor 105 [10 mM, CDCl ₃ /MeOD (7:3, v/v)], 298 K) with increasing equivalent of Hg ²⁺ (0-.8 equiv.) from bottom to the top	81
Figure 2.26	¹ H-NMR spectrum of compound 88	92
Figure 2.27	¹³ C-NMR spectrum of compound 88	92
Figure 2.28	HRMS(ES ⁺) spectrum of compound 88	93
Figure 2.29	¹ H-NMR spectrum of compound 89	93
Figure 2.30	¹³ C-NMR spectrum of compound 89	94
Figure 2.31	HRMS(ES ⁺) spectrum of compound 89	94
Figure 2.32	¹ H-NMR spectrum of compound 90	95
Figure 2.33	HRMS(ES ⁺) spectrum of compound 90	95
Figure 2.34	¹ H-NMR spectrum of compound 93	96
Figure 2.35	¹³ C-NMR spectrum of compound 93	96
Figure 2.36	HRMS-(ES ⁺) spectrum of compound 93	97
Figure 2.37	¹ H-NMR spectrum of compound 97a	97
Figure 2.38	¹³ C-NMR spectrum of compound 97a	98
Figure 2.39	HRMS(ES ⁺) spectrum of compound 97a	98

Figure 2.40	¹ H-NMR spectrum of compound 97b	99
Figure 2.41	¹³ C-NMR spectrum of compound 97b	99
Figure 2.42	HRMS(ES ⁺) spectrum of compound 97b	100
Figure 2.43	¹ H NMR spectrum of compound 100	100
Figure 2.44	¹³ C NMR spectrum of compound 100	101
Figure 2.45	HRMS (ES ⁺) spectrum of compound 100	101
Figure 2.46	¹ H spectrum of compound 103	102
Figure 2.47	¹³ C NMR spectrum of compound 103	102
Figure 2.48	¹ H spectrum of compound 104	103
Figure 2.49	¹³ C NMR spectrum of compound 104	103
Figure 2.50	HRMS (ES ⁺) spectrum of compound 104	104
Figure 2.51	¹ H NMR spectrum of compound 105	104
Figure 2.52	¹³ C NMR spectrum of compound 105	105
Figure 2.53	HRMS (ES ⁺) spectrum of compound 105	105
Figure 2.54	¹ H NMR titration binding isotherm for receptor 90 and chloride ion in CDCl ₃ ($K_a = 970 \text{ M}^{-1}$)	106
Figure 2.55	¹ H NMR titration binding isotherm for receptor 90 and bromide ion in CDCl ₃ ($K_a = 820 \text{ M}^{-1}$)	106
Figure 2.56	¹ H NMR titration binding isotherm for receptor 90 and fluoride ion in CDCl ₃ ($K_a = 600 \text{ M}^{-1}$)	107
Figure 2.57	¹ H NMR titration binding isotherm for receptor 90 and hydrogen sulphate ion in CDCl ₃ ($K_a = 410 \text{ M}^{-1}$)	107

Figure 2.58	^1H NMR titration binding isotherm for receptor 90 and iodide ion in CDCl_3 ($K_a = 170 \text{ M}^{-1}$)	108
Figure 2.59	^1H NMR titration binding isotherm for receptor 93 and hydrogen sulphate ion in CDCl_3 ($K_a = 210 \text{ M}^{-2}$)	109
Figure 2.60	^1H NMR titration binding isotherm for receptor 93 and chloride ion in CDCl_3 ($K_a = 150 \text{ M}^{-2}$)	109
Figure 2.61	^1H NMR titration binding isotherm for receptor 93 and fluoride ion in CDCl_3 ($K_a = 100 \text{ M}^{-2}$)	110
Figure 2.62	^1H NMR titration binding isotherm for receptor 97a and acetate ion in 20% DMSO in CDCl_3 ($K_a = 100 \text{ M}^{-1}$)	111
Figure 2.63	^1H NMR titration binding isotherm for receptor 97a and fluoride ion in 20% DMSO in CDCl_3 ($K_a = 60 \text{ M}^{-1}$)	111
Figure 2.64	^1H NMR titration binding isotherm for receptor 97a and chloride ion in 20% DMSO in CDCl_3 ($K_a = 45 \text{ M}^{-1}$)	112
Figure 2.65	^1H NMR titration binding isotherm for receptor 97a and bromide ion in 20% DMSO in CDCl_3 ($K_a = 30 \text{ M}^{-1}$)	112
Figure 2.66	^1H NMR titration binding isotherm for receptor 97b and acetate ion in 20% DMSO in CDCl_3 ($K_a = 70 \text{ M}^{-1}$).	113
Figure 2.67	^1H NMR titration binding isotherm for receptor 97b and fluoride ion in 20% DMSO in CDCl_3 ($K_a = 35 \text{ M}^{-1}$).	113
Figure 2.68	^1H NMR titration binding isotherm for receptor 97b and chloride ion in 20% DMSO in CDCl_3 ($K_a = 25 \text{ M}^{-1}$)	114
Figure 2.69	^1H NMR titration binding isotherm for receptor 97b and	114

	bromide ion in 20% DMSO in CDCl ₃ ($K_a = 20 \text{ M}^{-1}$).	
Figure 3.1	TEM image of AgNPs stabilized with (a) compound 38a , (b) compound 38b , (c) compound 38c , (d) compound 42a , (e) compound 42b , (f) compound 42c , respectively	137
Figure 3.2	(a) UV-Vis spectra of compound 42a stabilized Ag NPs before and after addition of Hg ²⁺ ion (0-84 μM); (b) TEM image of compound 42a stabilized Ag NPs after addition of Hg ²⁺ ion	139
Figure 3.3	Photographs of the solution of AgNPs stabilized with compound 38a after addition of metal ions and anions	140
Figure 3.4	Photographs of the solutions of AgNPs stabilized with compound 38b after addition of metal ions and anions	141
Figure 3.5	Photographs of the solutions of AgNPs stabilized with compound 38c after addition of metal ions and anions.	141
Figure 3.6	Photographs of the solutions of AgNPs stabilized with compound 42a after addition of metal ions and anions	142
Figure 3.7	Photographs of the solutions of AgNPs stabilized with compound 42b after addition of metal ions and anions	142
Figure 3.8	Photographs of the solutions of AgNPs stabilized with compound 42c after addition of metal ions and anions	143
Figure 3.9	¹ H NMR spectrum of 36a	152
Figure 3.10	¹³ C NMR spectrum of 36a	152
Figure 3.11	¹ H NMR spectrum of 36b	153
Figure 3.12	¹³ C NMR spectrum of 36b	153

Figure 3.13	^1H NMR spectrum of 36c	154
Figure 3.14	^{13}C NMR spectrum of 36c	154
Figure 3.15	^1H NMR spectrum of 37a	155
Figure 3.16	^{13}C NMR spectrum of 37a	155
Figure 3.17	^1H NMR spectrum of 37b	156
Figure 3.18	^{13}C NMR spectrum of 37b	156
Figure 3.19	^1H NMR spectrum of 37c	157
Figure 3.20	^{13}C NMR spectrum of 37c	157
Figure 3.21	^1H NMR spectrum of 38a	158
Figure 3.22	^{13}C NMR spectrum of 38a	158
Figure 3.23	HRMS (ES) $^+$ spectrum of 38a	159
Figure 3.24	^1H NMR spectrum of 38b	159
Figure 3.25	^{13}C NMR spectrum of 38b	160
Figure 3.26	HRMS (ES) $^+$ spectrum of 38b	160
Figure 3.27	^1H NMR spectrum of 38c	161
Figure 3.28	^{13}C NMR spectrum of 38c	161
Figure 3.29	HRMS (ES) $^+$ spectrum of 38c	162
Figure 3.30	^{13}C NMR spectrum of 41a	162
Figure 3.31	^{13}C NMR spectrum of 41a	163
Figure 3.32	^1H NMR spectrum of 41b	163
Figure 3.33	^{13}C NMR spectrum of 41b	164
Figure 3.34	^1H NMR spectrum of 41c	164
Figure 3.35	^{13}C NMR spectrum of 41c	165

Figure 3.36	^1H NMR spectrum of 42a	165
Figure 3.37	^{13}C NMR spectrum of 42a	166
Figure 3.38	HRMS (ES) $^+$ spectrum of 42a	166
Figure 3.39	^1H NMR spectrum of 42b	167
Figure 3.40	^{13}C NMR spectrum of 42b	167
Figure 3.41	HRMS (ES) $^+$ spectrum of 42b	168
Figure 3.42	^1H NMR spectrum of 42c	168
Figure 3.43	^{13}C NMR spectrum of 42c	169
Figure 3.44	HRMS (ES) $^+$ spectrum of 42c	169
Figure 4.1	Structures of flavin derivatives	172
Figure 4.2	Common redox and protonation states of the flavin cofactor	173
Figure 4.3	(a) Partial ^1H NMR titrations stacking plot of receptors 12a (10 mM, CDCl_3 , 298 K) with increasing equivalent of <i>N</i> (10)-hexylflavin (0-4.6 equiv.) from bottom to the top (b) Proposed binding mode between receptor 12a and <i>N</i> (10)-hexylflavin	181
Figure 4.4	(a) ^1H NMR titration binding isotherm for receptor 12a and <i>N</i> (10)-hexylflavin in CDCl_3 ($K_a = 3500 \text{ M}^{-1}$) (b) Jobs plot showing 1:1 complex formation between 12a and <i>N</i> (10)-hexylflavin	182
Figure 4.5	Partial ^1H NMR titrations stacking plot of receptors 12b (10 mM, CDCl_3 , 298 K) with increasing equivalent of <i>N</i> (10)-hexylflavin (0-4.6 equiv.) from bottom to the top	183
Figure 4.6	Partial ^1H NMR titrations stacking plot of receptors 12c (10 mM, CDCl_3 , 298 K) with increasing equivalent of <i>N</i> (10)-hexylflavin (0-4.6 equiv.) from bottom to the top	183

mM, CDCl₃, 298 K) with increasing equivalent of *N*(10)-hexylflavin (0-4.8 equiv.) from bottom to the top

Figure 4.7	Partial ¹ H NMR titrations stacking plot of receptors 12d (10 mM, CDCl ₃ , 298 K) with increasing equivalent of <i>N</i> (10)-hexylflavin (0-5.0 equiv.) from bottom to the top.	183
Figure 4.8	¹ H NMR spectrum of 3 α ,7 α ,12 α - <i>o</i> -triformylcholic acid	189
Figure 4.9	¹³ C NMR spectrum of 3 α ,7 α ,12 α - <i>o</i> -triformylcholic acid	189
Figure 4.10	¹ H NMR spectrum of 11	190
Figure 4.11	¹³ C NMR spectrum of 11	190
Figure 4.12	HRMS (ES ⁺) spectrum of 11	191
Figure 4.13	¹ H NMR spectrum of 12a	191
Figure 4.14	¹³ C NMR spectrum of 12a	192
Figure 4.15	HRMS (ES ⁺) spectrum of 12a	192
Figure 4.16	¹ H NMR spectrum of 12b	193
Figure 4.17	¹³ C NMR spectrum of 12b	193
Figure 4.18	HRMS (ES ⁺) spectrum of 12b	194
Figure 4.19	¹ H NMR spectrum of 12c	194
Figure 4.20	¹³ C NMR spectrum of 12c	195
Figure 4.21	HRMS (ES ⁺) spectrum of 12c	195
Figure 4.22	¹ H NMR spectrum of 12d	196
Figure 4.23	¹³ C NMR spectrum of 12d	196
Figure 4.24	HRMS (ES ⁺) spectrum of 12d	197
Figure 4.25	¹ H NMR titration binding isotherm for receptor 12b and	198

	<i>N</i> (10)- hexylflavin in CDCl ₃ ($K_a = 2000 \text{ M}^{-1}$)	
Figure 4.26	¹ H NMR titration binding isotherm for receptor 12c and <i>N</i> (10)-hexylflavin in CDCl ₃ ($K_a = 1000 \text{ M}^{-1}$)	198
Figure 5.1	Absorbance spectra of compound 14 ($1 \times 10^{-5} \text{ M}$) in CH ₃ CN in the presence of F ⁻ (0-1.2 equiv)	206
Figure 5.2	(a)Hildebrand-Benesi plot based on the 1:1 binding model: $A_0/(420 \text{ nm}) \cdot \chi$ versus $[G]^{-1}$; (b) Job's plot showing 1:1 complex formation between 14 and F ⁻	206
Figure 5.3	Absorbance spectra of compound 14 ($1 \times 10^{-5} \text{ M}$) in CH ₃ CN in the presence of H ₂ SO ₄ ⁻ (0-1.5 equiv)	207
Figure 5.4	(a)Hildebrand-Benesi plot based on the 1:1 binding model: $A_0/(420 \text{ nm}) \cdot \chi$ versus $[G]^{-1}$; (b) Job's plot showing 1:1 complex formation between 14 and H ₂ PO ₄ ⁻	207
Figure 5.5	A photograph of ($1 \times 10^{-5} \text{ M}$) solution of receptor 14 in CH ₃ CN and after addition of 0.4 equiv of F ⁻ , 5 equiv H ₂ PO ₄ ⁻ and 8 equiv of Cl ⁻ , Br ⁻ , I ⁻ , HSO ₄ ⁻ , CH ₃ COO ⁻	208
Figure 5.6	Partial ¹ H NMR spectra (300 MHz, CD ₃ CN, δ in ppm) of 14 showing chemical shift change in the presence of incremental addition of TBAF (0-1.2 equiv).	209
Figure 5.7	Absorbance spectra of compound 14 ($1 \times 10^{-5} \text{ M}$) in CH ₃ CN in the presence of Cu ²⁺ (0-1.2 equiv)	209

Figure 5.8	(a)Hildebrand-Benesi plot based on the 1:1 binding model: $A_0/(420 \text{ nm}) \cdot \chi$ versus $[G]^{-1}$; (b) Job's plot showing 1:1 complex formation between 14 and Cu^{2+}	210
Figure 5.9	A photograph of (1×10^{-4} M) solution of receptor 14 in CH_3CN and after addition of 0.2 equiv of Cu^{2+} and 5 equiv of other metals	211
Figure 5.10	Partial ^1H NMR spectra (300 MHz, CD_3CN , δ in ppm) of 14 showing chemical shift change in the presence of incremental addition of Cu^{2+} ion (0-0.8 equiv).	211
Figure 5.11	^1H -NMR spectrum of compound 12	214
Figure 5.12	^{13}C -NMR spectrum of compound 12	214
Figure 5.13	^1H -NMR spectrum of compound 13	215
Figure 5.14	^{13}C -NMR spectrum of compound 13	215
Figure 5.15	^1H -NMR spectrum of compound 14	216
Figure 5.16	^{13}C -NMR spectrum of compound 14	216
Figure 5.16	HRMS spectrum of compound 14	217

LIST OF TABLES

Figure No.	Description	Page No.
Table 2.1	Association constant K_a (M^{-1}) ^a for 1:1 complexes of receptors 90 -(PF ₆) ₂ with anions in CDCl ₃ at 298 K	57
Table 2.2	Association constant K_a (M^{-2}) ^a for 1:2 complexes of receptor 93 with anions in CDCl ₃ at 298 K	62
Table 2.3	Association constant K_a (M^{-1}) ^a for 1:1 complexes of receptors 97a and 97b with anions in 20% DMSO in CDCl ₃ at 298 K	66
Table 3.1	Average size of AgNPs stabilized with compounds 38a-c and 42a-c	137
Table 3.2	Minimum concentration of Hg ²⁺ ion detectable by the visual colour change with AgNPs stabilized with compounds 38a-c and 42a-c .	138
Table 4.1	Association constant K_a (M^{-1}) ^a for 1:1 complexes of 2,6-diaminopyridine based receptors 7a-c and 8a-b with <i>N</i> (10)-hexyl and <i>N</i> (10)-octyl flavins in CDCl ₃ at 298 K	177
Table 4.2	Association constants K_a (M^{-1}) ^a for 1:1 complexes of 2,6-diaminopyridine based receptors 12a-d with <i>N</i> (10)-hexylflavin in CDCl ₃ at 298 K	184

Glossary of symbols and Abbreviations

%	percentage
δ	chemical shift
$^{\circ}\text{C}$	degree centigrade
Ar	aryl
bs	broad singlet
CDCl_3	deuterated chloroform
CD_3OD	deuterated methanol
$\text{Cu}(\text{SO}_4)_2$	copper sulphate
d	doublet
DMF	<i>N,N'</i> -dimethylformamide
DMSO-d_6	deuterated dimethyl sulfoxide
g	gram
mp	melting point
h	hour
min.	minute
IR	infrared
<i>J</i>	coupling constant
m	multiplet
mg	milligram
K_a	association constant
MHz	megahertz

Hz	hertz
mmol	millimole
Soln	solution
M	molar
NMR	nuclear magnetic resonance
rt	room temperature
s	singlet
TLC	thin layer chromatography
TMS	tetramethylsilane
t	triplet
<i>m/z</i>	mass/charge
HRMS	high resolution mass spectrum
ESI	electrospray ionization
TEM	transmission electron microscopy
SEM	scanning electron microscopy
AgNP	silver nanoparticle

NOTES

1. All the melting points reported in the thesis were taken on an electrical melting point apparatus.
2. All the solvents were purified by routine methods and were distilled before use.
3. TLC was performed on silica gel plates using iodine for visualizing spots.
4. Purification of the compounds was done by flash chromatography using Spectrochem silica gel 60-120 mesh.
5. IR spectra were recorded on a Nicolet Protégé 460 FTIR Spectrometer, using potassium bromide pellets.
6. ^1H and ^{13}C NMR spectra were recorded on a Bruker Spectrospin DPX 300. Tetramethylsilane was used as internal reference and the chemical shifts are expressed as displacement (δ) in ppm downfield from tetramethylsilane.
7. High resolution mass spectra (ES) were recorded on a Bruker MicroTOF-Q II.
8. Absorption spectra were recorded on Perkin Elmer Lambda bio-20 double-beam spectrophotometer.
9. Fluorescence spectra were recorded on Horiba scientific fluoromax-4
10. SEM images were recorded on Carl Zeiss EVO 50 WDS electron microscope.
11. TEM images were recorded on Tecnai G² 20 electron microscope operated at 200 kV.